

Observation of $\bar{B}^0 \rightarrow D^0 \eta'$ and $\bar{B}^0 \rightarrow D^{*0} \eta'$

J. Schümann,²⁵ K. Abe,⁸ K. Abe,⁴¹ H. Aihara,⁴³ Y. Asano,⁴⁷ T. Aushev,¹² S. Bahinipati,⁴ A. M. Bakich,³⁸ Y. Ban,³² I. Bedny,¹ U. Bitenc,¹³ I. Bizjak,¹³ S. Blyth,²⁵ A. Bondar,¹ A. Bozek,²⁶ M. Bračko,^{8,19,13} J. Brodzicka,²⁶ T. E. Browder,⁷ M.-C. Chang,²⁵ P. Chang,²⁵ Y. Chao,²⁵ A. Chen,²³ W. T. Chen,²³ B. G. Cheon,³ R. Chistov,¹² S.-K. Choi,⁶ Y. Choi,³⁷ Y. K. Choi,³⁷ A. Chuvikov,³³ S. Cole,³⁸ J. Dalseno,²⁰ M. Dash,⁴⁸ S. Eidelman,¹ Y. Enari,²¹ F. Fang,⁷ N. Gabyshev,¹ A. Garmash,³³ T. Gershon,⁸ G. Gokhroo,³⁹ B. Golob,^{18,13} J. Haba,⁸ N. C. Hastings,⁸ K. Hayasaka,²¹ H. Hayashii,²² M. Hazumi,⁸ L. Hinz,¹⁷ T. Hokuue,²¹ Y. Hoshi,⁴¹ W.-S. Hou,²⁵ Y. B. Hsiung,²⁵ T. Iijima,²¹ A. Imoto,²² K. Inami,²¹ Y. Iwasaki,⁸ J. H. Kang,⁴⁹ J. S. Kang,¹⁵ N. Katayama,⁸ H. Kawai,² T. Kawasaki,²⁸ H. R. Khan,⁴⁴ H. Kichimi,⁸ H. J. Kim,¹⁶ S. M. Kim,³⁷ S. Korpar,^{19,13} P. Krokovny,¹ C. C. Kuo,²³ A. Kuzmin,¹ Y.-J. Kwon,⁴⁹ J. S. Lange,⁵ S. E. Lee,³⁶ S. H. Lee,³⁶ Y.-J. Lee,²⁵ T. Lesiak,²⁶ J. Li,³⁵ S.-W. Lin,²⁵ G. Majumder,³⁹ T. Matsumoto,⁴⁵ A. Matyja,²⁶ W. Mitaroff,¹¹ K. Miyabayashi,²² H. Miyake,³⁰ H. Miyata,²⁸ R. Mizuk,¹² T. Nagamine,⁴² Y. Nagasaka,⁹ E. Nakano,²⁹ M. Nakao,⁸ Z. Natkaniec,²⁶ S. Nishida,⁸ O. Nitoh,⁴⁶ S. Ogawa,⁴⁰ T. Ohshima,²¹ T. Okabe,²¹ S. Okuno,¹⁴ S. L. Olsen,⁷ W. Ostrowicz,²⁶ P. Pakhlov,¹² C. W. Park,³⁷ N. Parslow,³⁸ R. Pestotnik,¹³ L. E. Piilonen,⁴⁸ M. Rozanska,²⁶ H. Sagawa,⁸ Y. Sakai,⁸ N. Sato,²¹ T. Schietinger,¹⁷ O. Schneider,¹⁷ H. Shibuya,⁴⁰ A. Somov,⁴ N. Soni,³¹ R. Stamen,⁸ S. Stanič,^{47,*} M. Starič,¹³ K. Sumisawa,³⁰ T. Sumiyoshi,⁴⁵ S. Suzuki,³⁴ S. Y. Suzuki,⁸ O. Tajima,⁸ F. Takasaki,⁸ N. Tamura,²⁸ M. Tanaka,⁸ Y. Teramoto,²⁹ X. C. Tian,³² T. Tsukamoto,⁸ S. Uehara,⁸ K. Ueno,²⁵ S. Uno,⁸ G. Varner,⁷ K. E. Varvell,³⁸ S. Villa,¹⁷ C. H. Wang,²⁴ M.-Z. Wang,²⁵ M. Watanabe,²⁸ A. Yamaguchi,⁴² Y. Yamashita,²⁷ M. Yamauchi,⁸ Heyoung Yang,³⁶ Y. Yuan,¹⁰ L. M. Zhang,³⁵ Z. P. Zhang,³⁵ V. Zhilich,¹ and D. Žontar^{18,13}

(The Belle Collaboration)

¹*Budker Institute of Nuclear Physics, Novosibirsk*

²*Chiba University, Chiba*

³*Chonnam National University, Kwangju*

⁴*University of Cincinnati, Cincinnati, Ohio 45221*

⁵*University of Frankfurt, Frankfurt*

⁶*Gyeongsang National University, Chinju*

⁷*University of Hawaii, Honolulu, Hawaii 96822*

⁸*High Energy Accelerator Research Organization (KEK), Tsukuba*

⁹*Hiroshima Institute of Technology, Hiroshima*

¹⁰*Institute of High Energy Physics, Chinese Academy of Sciences, Beijing*

¹¹*Institute of High Energy Physics, Vienna*

¹²*Institute for Theoretical and Experimental Physics, Moscow*

¹³*J. Stefan Institute, Ljubljana*

¹⁴*Kanagawa University, Yokohama*

¹⁵*Korea University, Seoul*

¹⁶*Kyungpook National University, Taegu*

¹⁷*Swiss Federal Institute of Technology of Lausanne, EPFL, Lausanne*

¹⁸*University of Ljubljana, Ljubljana*

¹⁹*University of Maribor, Maribor*

²⁰*University of Melbourne, Victoria*

²¹*Nagoya University, Nagoya*

²²*Nara Women's University, Nara*

²³*National Central University, Chung-li*

²⁴*National United University, Miao Li*

²⁵*Department of Physics, National Taiwan University, Taipei*

²⁶*H. Niewodniczanski Institute of Nuclear Physics, Krakow*

²⁷*Nihon Dental College, Niigata*

²⁸*Niigata University, Niigata*

²⁹*Osaka City University, Osaka*

³⁰*Osaka University, Osaka*

³¹*Panjab University, Chandigarh*

³²*Peking University, Beijing*

³³*Princeton University, Princeton, New Jersey 08545*

³⁴*Saga University, Saga*

³⁵*University of Science and Technology of China, Hefei*

- ³⁶Seoul National University, Seoul
³⁷Sungkyunkwan University, Suwon
³⁸University of Sydney, Sydney NSW
³⁹Tata Institute of Fundamental Research, Bombay
⁴⁰Toho University, Funabashi
⁴¹Tohoku Gakuin University, Tagajo
⁴²Tohoku University, Sendai
⁴³Department of Physics, University of Tokyo, Tokyo
⁴⁴Tokyo Institute of Technology, Tokyo
⁴⁵Tokyo Metropolitan University, Tokyo
⁴⁶Tokyo University of Agriculture and Technology, Tokyo
⁴⁷University of Tsukuba, Tsukuba
⁴⁸Virginia Polytechnic Institute and State University, Blacksburg, Virginia 24061
⁴⁹Yonsei University, Seoul
(Dated: August 17, 2019)

We report the observation of $\bar{B}^0 \rightarrow D^0 \eta'$ and the first observation of $\bar{B}^0 \rightarrow D^{*0} \eta'$, using 140 fb⁻¹ of data collected at the $\Upsilon(4S)$ resonance with the Belle detector at the KEKB asymmetric energy e^+e^- collider. We find the branching fractions to be $\mathcal{B}(\bar{B}^0 \rightarrow D^0 \eta') = [1.14 \pm 0.20 \text{ (stat)} \pm_{-0.13}^{+0.10} \text{ (syst)}] \times 10^{-4}$ and $\mathcal{B}(\bar{B}^0 \rightarrow D^{*0} \eta') = [1.21 \pm 0.34 \text{ (stat)} \pm 0.22 \text{ (syst)}] \times 10^{-4}$ with significances including systematic uncertainty of 8.9 and 5.3 standard deviations, respectively.

The colour-suppressed decays $\bar{B}^0 \rightarrow D^{(*)0} h^0$ have been observed for $h^0 = \pi^0, \eta, \omega$ and ρ^0 [1, 2, 3, 4] and recently also $\bar{B}^0 \rightarrow D^0 \eta'$ [4]. The rates are all larger than originally expected in generalized factorization [5]. The large branching fractions may be explained by final state rescattering [6] or non-factorizable diagrams in perturbative QCD [7]. Hard-collinear effective theory [8] cannot explain the rate for $\bar{B}^0 \rightarrow D^{(*)0} \pi^0$; other decay modes have not been investigated in this framework.

Both the colour-allowed decay $\bar{B}^0 \rightarrow D^{(*)+} h^-$ [9] and the colour-suppressed decay $\bar{B}^0 \rightarrow D^{(*)0} h^0$ proceed via the emission of a virtual W^- . In the former case the W^- can decay without colour restrictions, however, in the latter case the d quark from the W^- decay has to carry colour that matches the colour of the \bar{d} quark originating from the \bar{B}^0 . This allows colour-singlet formation only in one out of three cases resulting in suppression by a factor of $\frac{1}{3}$ (therefore colour-suppressed). The tree level diagrams for both decays are shown in Fig. 1. The contribution of the W -exchange diagram is usually assumed to be negligible [5].

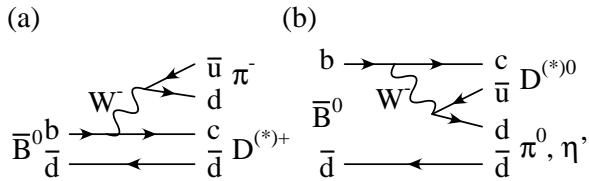


FIG. 1: Colour-allowed (a) and colour-suppressed (b) tree level Feynman diagrams for $\bar{B} \rightarrow D^{(*)} h$.

The branching fraction for $\bar{B}^0 \rightarrow D^0 \eta'$ and an upper limit for the $\bar{B}^0 \rightarrow D^{*0} \eta'$ decay have recently been published by BaBar [4]. In this Letter we present the first observation of $\bar{B}^0 \rightarrow D^{*0} \eta'$ and an observation of $\bar{B}^0 \rightarrow D^0 \eta'$ with more than 5Σ statistical significance.

This analysis is based on a 140 fb⁻¹ data sample containing 152×10^6 $B\bar{B}$ events collected with the Belle detector at the KEKB [10] e^+e^- collider. KEKB is an asymmetric energy collider (3.5 GeV on 8 GeV) that operates at the $\Upsilon(4S)$ resonance ($\sqrt{s} = 10.58$ GeV) with peak luminosity of nearly 1.4×10^{-34} cm⁻²s⁻¹. B^+B^- and $B^0\bar{B}^0$ pairs are assumed to be produced with equal rates. For signal and background simulation the QQ [11] Monte Carlo (MC) generator was used and the GEANT3 [12] package was used for detector simulation.

The Belle detector is a large-solid-angle magnetic spectrometer consisting of a three-layer silicon vertex detector (SVD), a 50-layer central drift chamber (CDC), an array of aerogel threshold Čerenkov counters (ACC), a barrel-like arrangement of time-of-flight scintillation counters (TOF), and an electromagnetic calorimeter comprised of CsI(Tl) crystals (ECL) located inside a superconducting solenoid coil that provides a 1.5 T magnetic field. An iron flux-return located outside of the coil is instrumented to detect K_L^0 mesons and to identify muons (KLM). The detector is described in detail elsewhere [13].

Charged tracks with impact parameters less than 0.5 cm radially and less than 2 cm in z (the z axis is anti-parallel to the positron beam direction) with respect to the interaction point and with momenta larger than 100 MeV/ c are selected. Kaon and pion mass hypotheses are assigned to charged tracks on the basis of a likelihood $\mathcal{L}_{K/\pi}$ that is obtained by combining information from the CDC (dE/dx), ACC and TOF systems. The likelihood ratio $\mathcal{R}_K = \mathcal{L}_K / (\mathcal{L}_\pi + \mathcal{L}_K)$ ranges between 0 (pion-like) and 1 (kaon-like) and we require $\mathcal{R}_K > 0.6$ for kaon and $\mathcal{R}_K < 0.4$ for pion candidates originating from the heavy meson yielding an efficiency of about 88% in both cases and $\mathcal{R}_K < 0.9$ for pion candidates from the light meson side corresponding to an efficiency of 99%. In addition, we reject tracks that are consistent with an electron or

muon hypothesis.

Photon candidates are selected with a minimum energy requirement of 50 MeV. Neutral pion candidates are reconstructed by combining two photons with invariant mass between 115 MeV/ c^2 and 152 MeV/ c^2 , which corresponds to ± 2.5 standard deviations in terms of the mass resolution. In addition, we require the momentum of the π^0 to be greater than 400 MeV/ c in the laboratory frame.

The η meson is reconstructed by combining two photons. An asymmetric η mass window was chosen, corresponding to $^{+2}_{-3}$ standard deviations. The mass of the η meson is then constrained to its nominal value from the Particle Data Group (PDG) [14].

We select ρ candidates from two oppositely charged pion candidate tracks in a mass region of $-220 \text{ MeV}/c^2 < M(\pi^+\pi^-) - m(\rho) < 170 \text{ MeV}/c^2$, where m_ρ is the nominal mass of ρ^0 mesons from the PDG and $M(\pi^+\pi^-)$ is the mass of the ρ candidate. In addition, we require the transverse momentum of the daughter pions, $P_T(\pi)$, to be greater than 300 MeV/ c . This requirement suppresses around 40% of the continuum background while retaining 86% of the signal candidates.

The η' meson is reconstructed in its two dominant decay channels $\eta' \rightarrow \eta\pi^+\pi^-$ and $\eta' \rightarrow \rho\gamma$. For both subdecays the η' candidates are required to be within a mass window of $0.94 \text{ GeV}/c^2 < M(\eta') < 0.975 \text{ GeV}/c^2$ and have a center-of-mass (CM) momentum of $P_{CM}(\eta') > 1.7 \text{ GeV}/c$. The pions from the η' decay must have a transverse momentum in the laboratory frame of $P_T(\pi) > 0.1 \text{ GeV}/c$. For the latter subdecay, the photon from the η' is required to have an energy greater than 0.2 GeV in the lab frame. This selection alone suppresses around 85% of background while retaining 85% of signal candidates. A weak requirement on the helicity of the η meson of $|h(\eta)| < 0.97$ is applied, where $h(\eta)$ is the cosine of the angle between the η' momentum and the direction of one of the decay photons in the η rest frame. An η' mass constraint is applied for the final fitting results.

The D^0 mesons are reconstructed in three different decay channels, $D^0 \rightarrow K^-\pi^+$, $D^0 \rightarrow K^-\pi^+\pi^0$ and $D^0 \rightarrow K^-\pi^+\pi^-\pi^+$ with mode-dependent $\pm 3\sigma$ mass windows. The $D^0 \rightarrow K^-\pi^+\pi^0$ decay channel has an additional requirement on the π^0 momentum of $P(\pi^0) > 0.4 \text{ GeV}/c$ in the lab frame to suppress continuum background. A D^0 mass constraint yields a significant improvement to the momentum resolution for the $D^0 \rightarrow K^-\pi^+\pi^0$ decay and is applied for all decay channels for consistency.

The D^{*0} mesons are reconstructed combining a D^0 meson with a π^0 or a γ . We require the mass difference of the D^0 and D^{*0} to satisfy $0.136 \text{ GeV}/c^2 < M(D^0\pi^0) - M(D^0) < 0.148 \text{ GeV}/c^2$ and $0.131 \text{ GeV}/c^2 < M(D^0\gamma) - M(D^0) < 0.156 \text{ GeV}/c^2$. In addition, we require the momentum of the D^0 in the lab frame to be greater than 0.8 GeV/ c .

The \bar{B}^0 mesons are reconstructed combining an η' me-

son and a D^0 or D^{*0} meson. Two kinematic variables are used to extract the \bar{B}^0 meson signal: the energy difference $\Delta E = E_B - E_{\text{beam}}$ and the beam constrained mass $M_{bc} = \sqrt{E_{\text{beam}}^2 - P_B^2}$, where E_{beam} is the beam energy and E_B and P_B are the reconstructed energy and momentum of the \bar{B}^0 candidate in the $\Upsilon(4S)$ rest frame. The events that satisfy the requirements $M_{bc} > 5.2 \text{ GeV}/c^2$ and $|\Delta E| < 0.25 \text{ GeV}$ are selected for further analysis.

After these selection criteria, the two major background sources are continuum $e^+e^- \rightarrow q\bar{q}$ (where $q = u, d, s, c$) and $b \rightarrow c$ decays.

Several event shape variables (defined in the CM frame) are used to distinguish the more spherical $B\bar{B}$ topology from the jet-like $q\bar{q}$ continuum events. The thrust angle θ_T is defined as the angle between the primary \bar{B}^0 decay daughters and the thrust axis formed by all tracks not from the same \bar{B}^0 meson. Jet-like events tend to peak near $|\cos\theta_T| = 1$, while spherical events have a flat distribution. The requirement $|\cos\theta_T| < 0.9$ is applied prior to any other event topology selections.

Additional continuum suppression is obtained by using modified Fox-Wolfram moments [15] and the angle θ_B between the flight direction of the reconstructed \bar{B}^0 candidate and the beam axis. A Fisher discriminant (\mathcal{F}) [16] is formed by a linear combination of $\cos\theta_T$, S_\perp and five modified Fox-Wolfram moments. S_\perp is the ratio of the scalar sum of the transverse momenta of all tracks outside a 45° cone around the η' direction to the scalar sum of their total momenta. Probability density functions (PDFs) are obtained from signal and background MC data samples. These variables are then combined to form a topological likelihood function $\mathcal{L}_c = \text{PDF}_c(\cos\theta_B) \cdot \text{PDF}_c(\mathcal{F})$ where $c = \text{signal (s) or continuum background (q}\bar{q})$. Signal follows a $1 - \cos^2(\theta_B)$ distribution while continuum background is uniformly distributed in $\cos\theta_B$. We select signal-like events by requiring a high likelihood ratio $\mathcal{R}_\mathcal{L} = \mathcal{L}_s/(\mathcal{L}_s + \mathcal{L}_{q\bar{q}})$ to suppress continuum background. For channels with an $\eta' \rightarrow \rho^0\gamma$ decay an additional variable $\cos\theta_H$, which is the angle between the η' momentum and the direction of one of the decay pions in the ρ rest frame, is included for better signal-background separation. The $\mathcal{R}_\mathcal{L}$ requirements are optimized using signal and continuum background Monte Carlo samples and are found to be strongly mode dependent and ranging from 0.1 to 0.925, where in general more restrictive constraints are applied for decays with $\eta' \rightarrow \rho^0\gamma$ and looser constraints for decays including a D^{*0} .

For events with multiple \bar{B}^0 candidates, the best candidate is selected on the basis of the χ^2 for the vertex fit to the charged pions from the η' . If multiple $D^{(*)}$ meson candidates remain after this selection, the best candidate is selected using $\chi^2 = (M(D^{(*)}) - m_{D^{(*)}})^2/\sigma^2$, where $M(D^{(*)})$ is the $D^{(*)}$ candidate mass, $m_{D^{(*)}}$ is the nominal $D^{(*)}$ mass and σ is the resolution of reconstructed $D^{(*)}$ mass. Multiple candidates in the heavy meson side

appear for less than 2% of the events for the $\bar{B}^0 \rightarrow D^0 \eta'$ decay but in the order of 20% for the $\bar{B}^0 \rightarrow D^{*0} \eta'$ decay.

Backgrounds from other B decay modes such as $B^- \rightarrow D^{(*)0} \rho^-$ and $B^- \rightarrow D^{(*)0} a_1^-$ are studied. These decays are suppressed by vetoing events where the ρ or a_1 could be constructed from the \bar{B}^0 candidate daughters with $-0.1 \text{ GeV} < \Delta E < 0.08 \text{ GeV}$ and $M_{bc} > 5.27 \text{ GeV}/c^2$. The vetos suppress about 10%–30% of the $B\bar{B}$ background after the final selection criteria, while retaining over 98% of the signal MC events. For decays with $\eta' \rightarrow \eta \pi^+ \pi^-$, which have less background contamination, the remaining $B\bar{B}$ contributions are modeled with a single two-dimensional smooth function, obtained from a large MC sample. For decays with $\eta' \rightarrow \rho^0 \gamma$ we divide these backgrounds into two groups, the $B^- \rightarrow D^{(*)0} a_1^-$ decays and all others, both are again modeled with two-dimensional smoothed histograms.

The signal PDFs are represented by a Gaussian plus a bifurcated Gaussian (a Gaussian with different width on either side of the mean) in ΔE and a bifurcated Gaussian in M_{bc} . All PDFs are extracted from Monte Carlo simulations. For $\bar{B}^0 \rightarrow D^0 \eta'$ events the feeddown from $\bar{B}^0 \rightarrow D^{*0} \eta'$ is modeled using 2-dimensional smoothed histograms. Continuum events are represented by a first or second order polynomial in ΔE and an empirical background function introduced by ARGUS [17] for M_{bc} . Signals should peak around $\Delta E = 0 \text{ GeV}$ and $M_{bc} = 5.28 \text{ GeV}/c^2$. Correction factors accounting for the difference between MC and data, determined from a study of the high statistics decay mode $\bar{B}^0 \rightarrow \eta' K_S$, are applied to the mean and width values of the signal shapes for both ΔE and M_{bc} .

The reconstruction efficiencies are determined from a large sample of signal MC events, and range from 0.6% – 11.2% for the 18 different decay channels, where the subdecay branching fractions are not included. Correction factors due to differences between data and MC are applied for the charged track identification, photon, π^0 and η reconstruction.

The signal yields (N_S) are extracted using extended unbinned maximum-likelihood fits simultaneously performed in ΔE and M_{bc} . An extended likelihood function is:

$$L(N_S, N_{B_j}) = \frac{e^{-(N_S + \sum_j N_{B_j})}}{N!} \prod_{i=1}^N \left[N_S P_S(\vec{x}_i) + \sum_j N_{B_j} P_{B_j}(\vec{x}_i) \right] \quad (1)$$

where N is the total number of events, i is and index running over the events, \vec{x}_i is a vector of the ΔE and M_{bc} values for each event and P_S and P_{B_j} are the probability density functions for signal and background, respectively, and the index j runs over all background sources. The signal yield N_S and background contents N_{B_j} are determined by maximizing the $L(N_S, N_{B_j})$ function in the (N_S, N_{B_j}) manifold, where the N_{B_j} defines a

j -dimensional submanifold of all different backgrounds. The statistical significance of the signal is calculated as $\Sigma = \sqrt{2 \ln(L_{\max}/L_0)}$, where L_{\max} and L_0 denote the maximum likelihood value and the likelihood value at zero branching fraction, respectively.

The signal and background normalisations are floated in the fit while other PDF parameters are fixed to values determined from MC studies. When combining two or more modes we fit for a common branching fraction instead of the signal yield for each mode. In the case of $\bar{B}^0 \rightarrow D^0 \eta'$, the contributions from the D^{*0} feeddown are fixed to the branching fraction obtained in this analysis and the number of D^{*0} events is calculated with a mode dependent “feeddown-efficiency”, which is derived from MC simulations of $\bar{B}^0 \rightarrow D^{*0} \eta'$ decays reconstructed as $\bar{B}^0 \rightarrow D^0 \eta'$. The branching fractions together with the yields, the reconstruction efficiency for each decay and the significances are listed in Table I. The ΔE and M_{bc} projections of the fits are shown in Fig. 2.

TABLE I: Signal yields, efficiencies ($= \sum_i \epsilon_i \mathcal{B}(D_i^{(*)})$, with the index i running over the $D^{(*)}$ subdecay modes), branching fractions \mathcal{B} and significances Σ .

Decay mode	Yield	Efficiency ($\times 10^{-4}$)	\mathcal{B} ($\times 10^{-4}$)	Σ
$\bar{B}^0 \rightarrow D^0 \eta'$	49.4 ± 8.7	28.3 ± 0.8	$1.14 \pm 0.20^{+0.10}_{-0.13}$	8.9
$\bar{B}^0 \rightarrow D^{*0} \eta'$	24.3 ± 6.8	13.0 ± 0.4	$1.21 \pm 0.34 \pm 0.22$	5.3

The major sources contributing to the systematic uncertainty of the branching fraction measurements are the systematics of the correction factors for the ΔE and M_{bc} shape parameters (1.9% – 3.4%, depending on the decay mode considered), the choice of the two-dimensional smooth functions (4.1% – 12.5%, this is estimated by fitting the data sample with one-dimensional functions instead, half the deviation is taken as the error, this systematic error partly includes the systematics from the PDFs) and the uncertainty of the reconstruction efficiency of charged tracks (1.0% per track). Other systematic error contributions are the uncertainty of the shape of the PDFs, which is quantified by varying each parameter of the PDFs by $\pm 1\sigma$ of its nominal value. The changes in the yield are added in quadrature, resulting in an error of 0.9% – 1.8%. The uncertainties in the reconstruction efficiencies for all η , π^0 and photons together give a systematic error in the range of 2.9% – 3.8%. The particle identification fake rate and efficiency uncertainties for all charged tracks yield a systematic error of up to 0.4%. The efficiency is estimated from MC data samples with an accuracy of 2.5% – 5.0%. By requiring different \mathcal{R}_C selection criteria the systematic error from this source is evaluated to be 2.0% – 8.9%. The subdecay branching fraction uncertainties as listed by the PDG [14] result in an error of 1.5% – 3.3% and the number of $B\bar{B}$ events

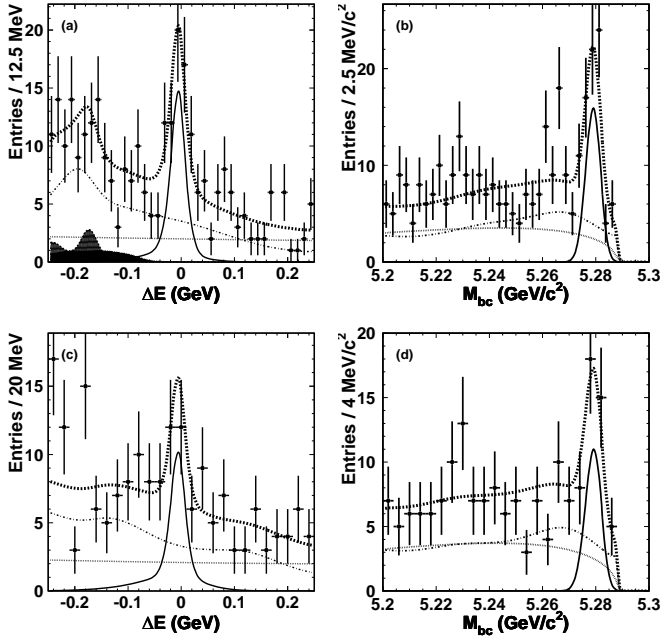


FIG. 2: $\bar{B}^0 \rightarrow D^0 \eta'$ decay ΔE (a) and M_{bc} (b) projection plots and $\bar{B}^0 \rightarrow D^{*0} \eta'$ decay ΔE (c) and M_{bc} (d) projection plots. Points with error bars represent the data, the solid line is the signal contribution, the dash-dotted line is $B\bar{B}$ and the dotted line is continuum background. The two shaded areas represent the $D^{*0} \rightarrow D\pi^0$ (dashed line, filled area) and $D^{*0} \rightarrow D\gamma$ (dotted line, hatched area) feeddown. The dashed line is the sum of all contributions. The projection plots are for signal regions of all other variables, the signal regions for ΔE and M_{bc} are: $-0.055 \text{ GeV} < \Delta E < 0.05 \text{ GeV}$ and $5.27 \text{ GeV} < M_{bc} < 5.29 \text{ GeV}$.

that are recorded with the Belle detector is known to an accuracy of 1%. The systematic error contributions described above are added in quadrature and result in a total systematic error of $^{+8.6}_{-11.5}\%$ for $\bar{B}^0 \rightarrow D^0 \eta'$ and $^{+18.1}_{-18.2}\%$ for $\bar{B}^0 \rightarrow D^{*0} \eta'$.

In summary, we observe the decays $\bar{B}^0 \rightarrow D^0 \eta'$ and $\bar{B}^0 \rightarrow D^{*0} \eta'$ with significances including systematic uncertainty of 8.9 and 5.3 standard deviations, respectively. The latter is observed for the first time. Our branching fraction for $\bar{B}^0 \rightarrow D^0 \eta'$ is about one standard deviation below another recent measurement [4]. Both branching fractions are higher than early theoretical predictions but are in agreement with recent work [7].

We thank the KEKB group for the excellent operation of the accelerator, the KEK Cryogenics group for the ef-

ficient operation of the solenoid, and the KEK computer group and the NII for valuable computing and Super-SINET network support. We acknowledge support from MEXT and JSPS (Japan); ARC and DEST (Australia); NSFC (contract No. 10175071, China); DST (India); the BK21 program of MOEHRD and the CHEP SRC program of KOSEF (Korea); KBN (contract No. 2P03B 01324, Poland); MIST (Russia); MESS (Slovenia); Swiss NSF; NSC and MOE (Taiwan); and DOE (USA).

* on leave from Nova Gorica Polytechnic, Nova Gorica

- [1] Belle Collaboration, K. Abe *et al.*, Phys. Rev. Lett. **88**, 052002 (2002).
- [2] Belle Collaboration, A. Satpathy *et al.*, Phys. Lett. B **553**, 159 (2003).
- [3] CLEO Collaboration, S. Ahmed *et al.*, Phys. Rev. D **66**, 031101 (2002).
- [4] BaBar Collaboration, B. Aubert *et al.*, Phys. Rev. D **69**, 032004 (2004).
- [5] M. Neubert and B. Stech, in *Heavy Flavours*, 2nd edition, ed. by A.J. Buras and M. Lindner (World Scientific, Singapore, 1998), p. 294.
- [6] C.-K. Chua and W.-S. Hou, Phys. Rev. D **65**, 096007 (2001).
- [7] C.-D. Lüe, Phys. Rev. D **68**, 097502 (2003).
- [8] S. Mantry *et al.*, plenary talk, hep-ph/0401058.
- [9] Throughout this paper, the inclusion of the charge conjugate mode decay is implied unless otherwise stated.
- [10] S. Kurokawa and E. Kikutani, Nucl. Instr. Meth., A **499**, 1 (2003), and other papers included in this Volume.
- [11] The event generator for B meson decay “QQ” was developed by the CLEO collaboration. <http://www.lns.cornell.edu/public/CLEO/soft/qq> (unpublished).
- [12] R. Brun, R. Hagelberg, M. Hanrout and J. C. Lassalle, CERN-DD-78-2-REV (1978).
- [13] Belle Collaboration, A. Abashian *et al.*, Nucl. Instr. Meth. A **479**, 117 (2002).
- [14] S. Eidelman *et al.*, Phys. Lett. B **592**, 1 (2004).
- [15] The Fox-Wolfram moments were introduced in G. C. Fox and S. Wolfram, Phys. Rev. Lett. **41**, 1581 (1978). The Fisher discriminant used by Belle, based on modified Fox-Wolfram moments, is described in K. Abe *et al.* (Belle Collab.), Phys. Rev. Lett. **87**, 101801 (2001) and K. Abe *et al.* (Belle Collab.), Phys. Lett. B **511**, 151 (2001).
- [16] R. A. Fisher, Annals of Eugenics **7**, 179 (1936).
- [17] The functional form is $x\sqrt{1-x^2}\exp[\alpha(1-x^2)]$, where $x = M_{bc}/E_{\text{beam}}$. ARGUS Collaboration, H. Albrecht *et al.*, Phys. Lett. B **241**, 278 (1990); **254**, 288 (1991).